HIGH-CONDUCTING LEAD-DOPED REDUCED GRAPHENE OXIDE (Pb$_x$:rGO$_{1-x}$) (0.4≤X≤0.6) COMPOSITES: SYNTHESIS, OPTICAL STUDY AND IONIC TRANSPORT CHARACTERISTICS FOR OPTOELECTRONIC APPLICATION.

[1]Ngari, A. Z., [1]Alpha, M., [1]Rabiu, B. M., [1]Muhammad, J., [1]Umar, M. M., [2]Daniel, T. O., [1]Idris, A. S. and [1]Adeyeba, O. A.

[1]Department of Physics, Nigerian Army University, Biu, Nigeria.
[2]Department of Physics, Alex Ekwueme-Federal University, Ndufu-Alike, Nigeria.

*Correspondence: alpha.matthew@naub.edu.ng   +2348062459364.

ABSTRACT

This research was centred on the study of the optical and ionic transport characteristics of charge carriers in the Pb doped reduced graphene oxide composite for optoelectronic application. Hummer's method and hydrothermal reduction methods were employed in the synthesis of the composites. For sample characterisation, energy dispersive x-ray spectroscopy, scanning electron microscopy (SEM), UV Spectrophotometer analysis, four-point Probe measurement and Hall Effect measurement were used to study the chemical compositions of the composite, its morphology, its optical characteristics and the ionic transport characteristics respectively. The SEM image demonstrates how the surface coalescence breaks down with increasing dopant concentration by a slight growth in the number of grain boundaries. However, due to the fact that every samples were synthesised under the same conditions, regardless of the amount of doping, every doped composite had a very similar microstructure and surface morphology. The rGO, Pb$_{0.4}$:rGO$_{0.6}$, and Pb$_{0.6}$:rGO$_{0.4}$ have band gaps of 1.4 eV, 1.6 eV, and 1.8 eV, respectively. The ionic conductivities (electrical conductivity due to the motion of ionic charge) for rGO, Pb$_{0.4}$:rGO$_{0.6}$, and Pb$_{0.6}$:rGO$_{0.4}$ composites were determined to be 0.001341 $\Omega^{-1}m^{-1}$, 0.002368 $\Omega^{-1}m^{-1}$, and 0.002745 $\Omega^{-1}m^{-1}$ respectively. The average Hall coefficient (R$_H$) values for the rGO, Pb$_{0.4}$:rGO$_{0.6}$, and Pb$_{0.6}$:rGO$_{0.4}$ composites, respectively, are 3.12 X 10^3 m^3/C, 2.57 X 10^3 m^3/C, and 2.88 X 10^3 m^3/C.

Keywords: Ionic Transport Characteristics, optoelectronic, Optical, Conductivity, Doping.

INTRODUCTION

This Study was centred on investigation of the optical and ionic transport characteristics of charge carriers in the Pb doped reduced graphene oxide composite for optoelectronic application. Due to their notable qualities, including stabilization, anti-corrosive properties, simple acid/base doping/de-doping, being light-weight, and also being comparatively inexpensive for composite preparation, reduced graphene oxide (rGO) nano-composites have attained a unique significance in both scientific research and academia (Alpha *et al*., 2019; Raymundo-Pinero *et al*., 2004; Martinelli *et al*., 2009). Depending on how much charge is transferred and their method of production, they demonstrate considerable improvement in their structures (Ilican *et al*., 2008; Largeot *et al*., 2008). In a range of technical applications, such as sensors, electrodes for supercapacitors, and optoelectronics,

Pb ions have most frequently been employed in various composites with carbonaceous materials. The objective of this research is to Study the optical and ionic transport characteristics of charge carriers in the composite for optoelectronic application. Graphene, which has a variety of applications and highly unique characteristics, is one such material that has attracted a great deal of attention since its discoveries. In order to enhance conducting active materials and produce fascinating electronic features by morphological modification and electronic interaction among constituents, Pb and rGO are mixed in various doping concentrations. Although there are a variety of techniques to synthesize rGO composites, hydrothermal reduction process is one typical method that is widely used. This method is employed to fabricate the composites used in this study. Energy dispersive x-ray spectroscopy,

133

scanning electron microscopy (SEM), a UV Spectrophotometer analysis, Four point Probe measurement and Hall Effect measurement were used to study the chemical compositions of the composite, its morphology, its optical characteristics and the ionic transport characteristics respectively.

The Hall Effect is observable when a magnetic field is passed through a sample and current is run along its length. This produces an electrical current that is perpendicular to the magnetic field and the current, which in turn produces a transverse voltage that is perpendicular to the field and the current. The Lorentz force, or the force that electromagnetic fields exert on a point charge, is the basis of this theory. Hall Effect measurements are incredibly useful for characterizing semiconductor materials, whether they are silicon-based, compound semiconductors, thin-film materials for solar cells, or nanoscale materials like graphene. Hall Effect measurement offers vast new opportunities for investigating charge carriers in continuum and quantum regimes. The optical Hall Effect can be conveniently exploited to characterize the electrical properties of materials (Mathias *et al*., 2016). The average crystallite size (D) is given as (Mukherjee and Mitra, 2015).

$$D = \frac{0.9\lambda}{\beta cos\theta} \qquad (1)$$

Where θ is the diffraction angle, λ the wavelength of the X-rays (1.5406 $^\circ$A) and β the full width at half maximum (FWHM). The absorption coefficient α is obtained using (Mukherjee and Mitra, 2015);

$$\alpha = 2.303\frac{A}{t} \qquad (2)$$

According to Jeyaprakash *et al*., (2010), the Tauc plot shows a relationship between the absorption coefficient and optical band gap E_g,

$$(\alpha h v)^{\frac{1}{p}} = A(hv - E_g) \qquad (3)$$

By extrapolating a straight line from the $(\alpha hv)^2$ vs. optical band gap plots to the $(\alpha hv)^2 = 0$ axis, where the intersection point gives the optical band gap, we were able to determine the optical band gap (E_g) of rGO, $Pb_{0.4}:rGO_{0.6}$, and $Pb_{0.6}:rGO_{0.4}$.

METHODOLOGY
SYNTHESIS OF REDUCED GRAPHENE OXIDE (rGO)

5 g of graphite was measured and another 2.5 g of sodium nitrate were added together. 115 ml of concentrated sulfuric acid was added to the mixture and sonicated at 60 ^{0}C for thirty minutes. The mixture was then transferred into an ice bathe, then 15 g of potassium permanganate was added slowly into the mixture and the temperature was maintained at below 20 ^{0}C, after the potassium permanganate was added, the temperature was then raised to 35 ^{0}C by sonication process for 20 min. 100 ml of distilled water and 1 g of ascorbic acid was added to the mixture slowly to aid reduction and the temperature was raised to 95 ^{0}C, then it was stirred for another 15 min. At the end of the 15 min, 100 ml of distilled water and 10 ml of hydrogen peroxide was added to the mixture to aid homogeneity. The solution was then filtered and then washed with 1 M of hydrochloric acid (8.3 ml of hydrochloric acid mixed with 100 ml of distilled water gives 1 M) and 100 ml of distilled water. The residue was then mixed with polyvinyl chloride and 4 drops of toluene were used to bind the residue, it was then placed on slides in an electric oven at 60 ^{0}C for 8 hrs to dry, and graphene oxide was obtained.

SYNTHESIS OF LEAD DOPED REDUCED GRAPHENE OXIDE ($Pb_x:rGO_{1-x}$) ($0.4 \leq X \leq 0.6$)

Pb_2CO_3 which serves as source for Pb and rGO were added to 100 ml of distilled water for the synthesis of $Pb_x:rGO_{1-x}$

134

(0.4≤x≤0.6) composite in the following compositions: $Pb_{0.4}:rGO_{0.6}$, $Pb_{0.6}:rGO_{0.4}$. The rGO cake was thoroughly grounded using an agate mortar and pestle, the mixture for each composition was sonicated for 30 min at 60 ^{0}C, after which it was transferred into a stainless-steel autoclave for hydrothermal reaction at 160 ^{0}C for 6 hrs. The pH was adjusted to neutral value using 50 ml of 0.1 M potassium hydroxide (1.12 g of potassium hydroxide diluted with 200 ml distilled water). The final product was collected filtered and washed with distilled water. The mixtures was then mixed with polyvinyl chloride and 4 drops of toluene and was placed on glass slides, the composite was then dried in an electric oven at 60 ^{0}C for 2 hrs. After it was dried, a composite of $Pb_x:rGO_{1-x}$ (0.4≤x≤0.6) was obtained.

SEM RESULTS

Figures 1, 2, and 3 display the SEM images and EDXs of rGO, $Pb_{0.4}:rGO_{0.6}$, and $Pb_{0.6}:rGO_{0.4}$, respectively. The morphology and microstructure of all samples in this investigation were analysed using a Phenoworld Pro X Model scanning electron microscope (SEM) operating in secondary electron detection mode at 2 kV.
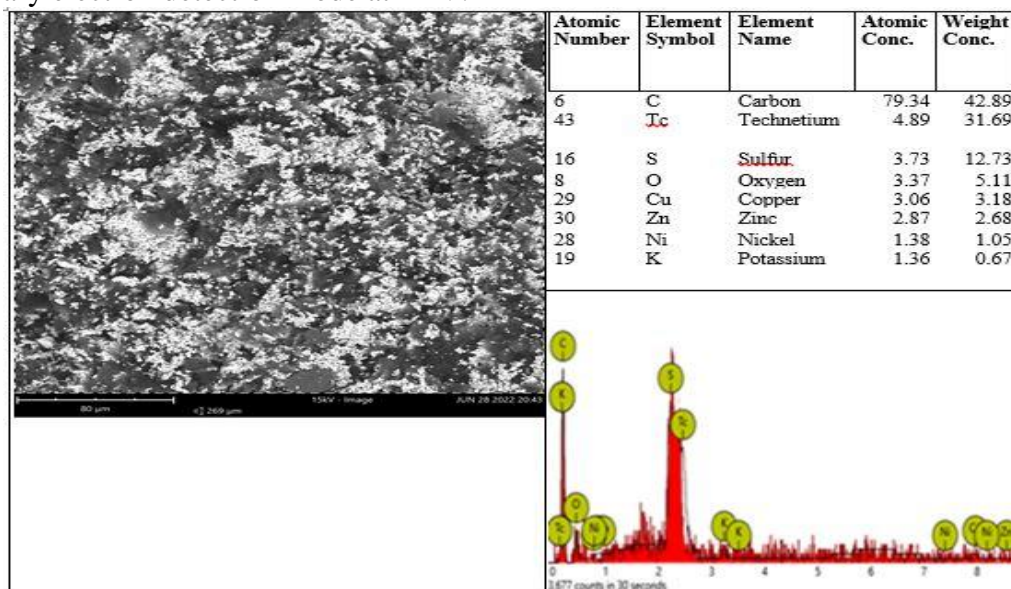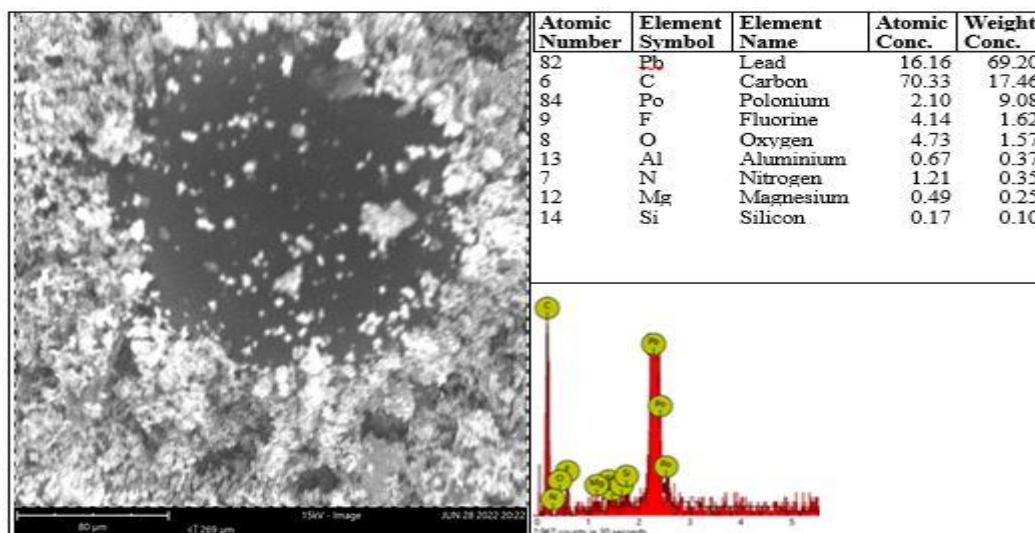
Atomic Number	Element Symbol	Element Name	Atomic Conc.	Weight Conc.
6	C	Carbon	79.34	42.89
43	Tc	Technetium	4.89	31.69
16	S	Sulfur	3.73	12.73
8	O	Oxygen	3.37	5.11
29	Cu	Copper	3.06	3.18
30	Zn	Zinc	2.87	2.68
28	Ni	Nickel	1.38	1.05
19	K	Potassium	1.36	0.67

Figure 1: SEM Image and EDX for rGO

Atomic Number	Element Symbol	Element Name	Atomic Conc.	Weight Conc.
82	Pb	Lead	16.16	69.20
6	C	Carbon	70.33	17.46
84	Po	Polonium	2.10	9.08
9	F	Fluorine	4.14	1.62
8	O	Oxygen	4.73	1.57
13	Al	Aluminium	0.67	0.37
7	N	Nitrogen	1.21	0.35
12	Mg	Magnesium	0.49	0.25
14	Si	Silicon	0.17	0.10

Figure 2: SEM Image and EDX for $Pb_{0.6}$:$rGO_{0.4}$

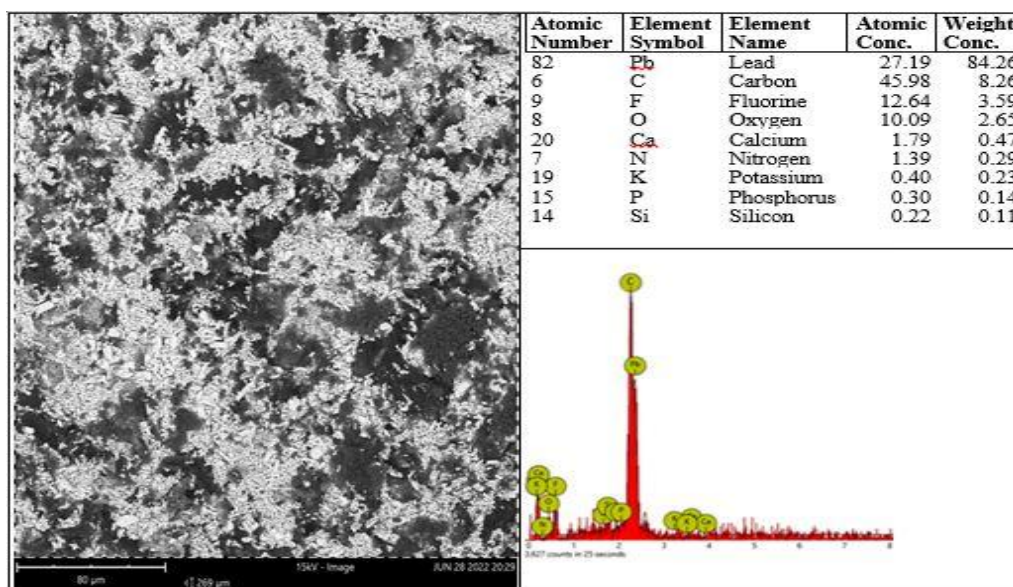| Atomic Number	Element Symbol	Element Name	Atomic Conc.	Weight Conc.
82	Pb	Lead	27.19	84.26
6	C	Carbon	45.98	8.26
9	F	Fluorine	12.64	3.59
8	O	Oxygen	10.09	2.65
20	Ca	Calcium	1.79	0.47
7	N	Nitrogen	1.39	0.29
19	K	Potassium	0.40	0.23
15	P	Phosphorus	0.30	0.14
14	Si	Silicon	0.22	0.11

Figure 3: SEM Image and EDX for $Pb_{0.6}$:$rGO_{0.4}$

The doped Pb atoms are chemically bounded between the layers of the reduced graphene oxide, as seen in the SEM image in figures 2 and 3, forming a composite material with excellent dispersion.

The doped composites revealed impressively consistent porous surface patterns, which are seen to grow with increasing doping concentrations. The SEM image demonstrates how the surface coalescence breaks down with increasing dopant concentration by a slight growth in the number of grain boundaries. However, due to the fact that every samples were synthesised under the same conditions, regardless of the amount of doping, every doped composite had a very similar microstructure and surface morphology. The interaction of reduced graphene oxide layers through van der Waals forces (Pandolfo and Hollenkamp, 2006;), which create a porous structure that allows electrolyte ions to easily access the surfaces of the composite, is what allows for the improved electrochemical utilization of Pb nanoparticles into the system of the reduced graphene oxide.
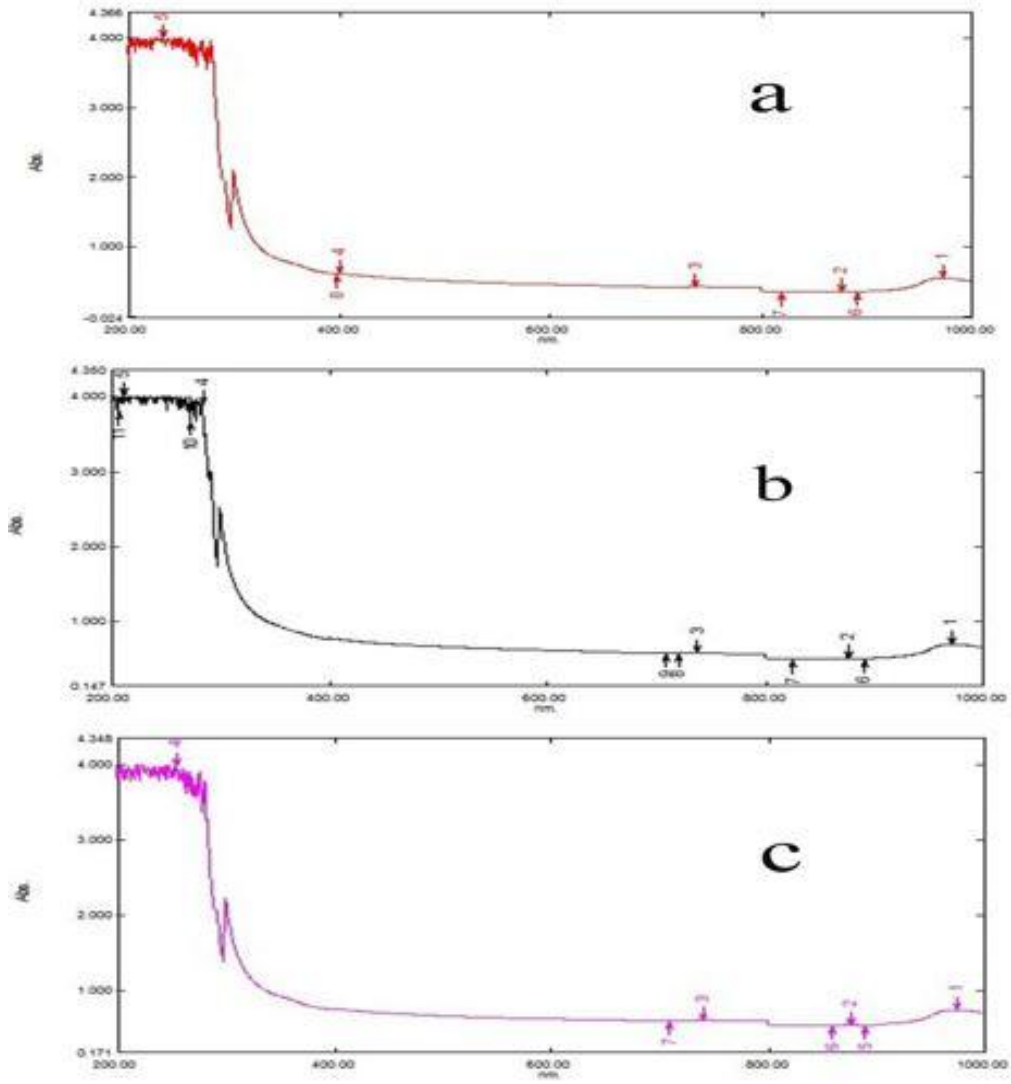
136

RESULTS AND DISCUSSION ON OPTICAL PROPERTIES

Figure 4: UV Spectra: (a) rGO; (b) $Pb_{0.4}$:$rGO_{0.6}$; (c) $Pb_{0.6}$:$rGO_{0.4}$
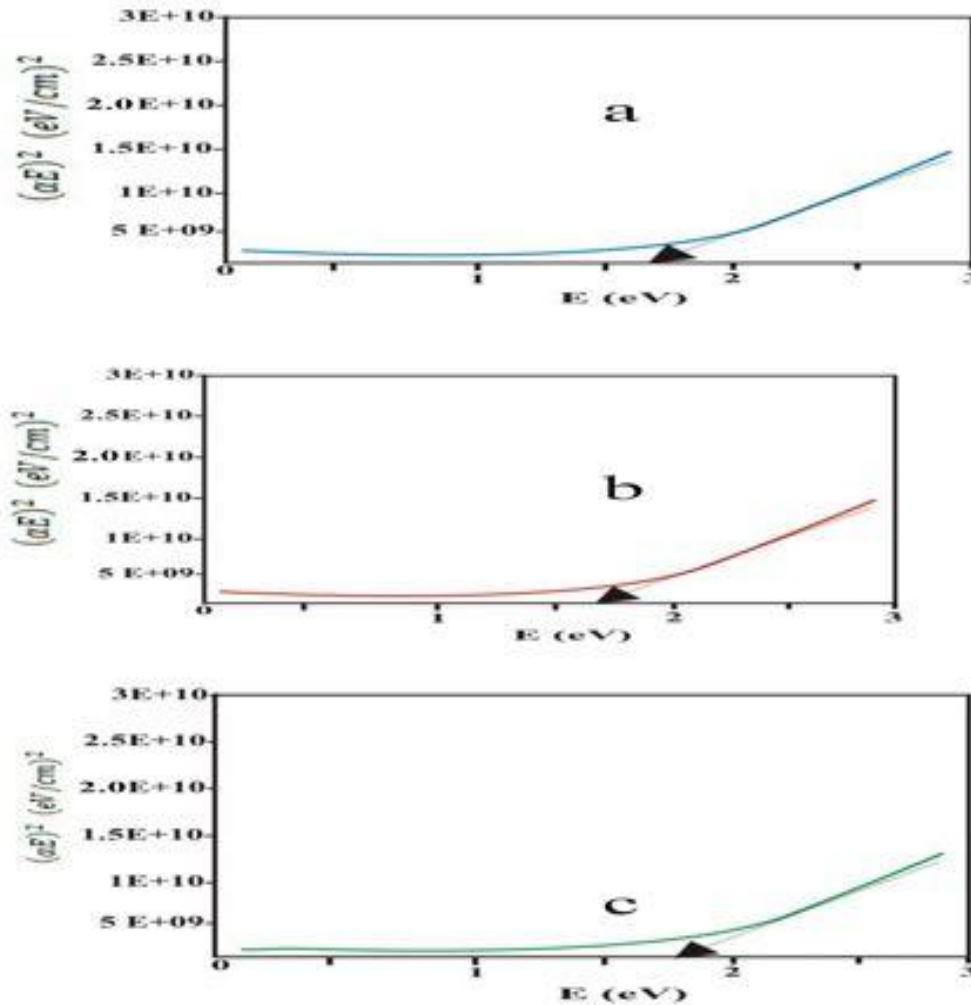
Figure 5: Tauc Plot: for (a) rGO; (b) $Pb_{0.4}$:rGO$_{0.6}$; (c) $Pb_{0.6}$:rGO$_{0.4}$

The shifts in peak as observed in figure 4 was due to the normalization condition. Smaller particle sizes are nearer to the shorter blue wavelength of light, or blue-shifted, whereas larger particle sizes are nearer to the longer wavelength of light, or red-shifted. The chromophore-related functional groups' transfer of electrons from the ground state to the excited state is what causes the red- and blue-shifted images to appear (Skoog *et al*., 2016; Uwe and Neil, 2011). According to the type of electrons contained in the composite material, electron excitation that takes place in UV-VIS spectrophotometry is recorded in the form of a spectra expressed as wavelength versus absorbance. From figure 4, the higher the absorbance, the more electrons are excited. Because there are more particles produced when Pb is doped, the optical density decreases as particle size increases. The ionic Pb is reduced and self-nucleates to produce new particles as the Pb ions are liberated from the surface.

The Tauc's plot, from which the optical band gap (Eg) was determined, is shown in Figure 5. The rGO, $Pb_{0.4}$:rGO$_{0.6}$, and $Pb_{0.6}$:rGO$_{0.4}$ have band gaps of 1.4 eV, 1.6 eV, and 1.8 eV, respectively. A similar observation was made by (Uwe and Neil, 2011; Daniel, *et al*., 2019), who also noted that the rise in the band gap was caused by an increase in ion concentration in the network of the composite material

RESULT AND DISCUSSION ON IONIC TRANSPORT CHARACTERISTICS

138

The results of the studies on the Hall Effect can be used to calculate the parameters of the conductivity type, Hall voltage, mobility, and carrier density. To build photovoltaic and optoelectronic devices with efficient charge separation and transistor switching, it is also essential to quantify the mobility of charge carriers (Kasap and Capper, 2017; Rajyalakshmi *et al*., 2020). The Hall Effect study was carried out using the Van der Pauw method and a uniquely engineered Hall four probe with Hall Effect configuration. This the Van der Pauw method employs a four-point probe, place around the perimeter of the sample. This method gives the average resistivity of the sample. Hall voltage was determined by applying a magnetic field of 0.25 T and increasing the samples' current in steps of 0.3 mA while they were at room temperature. As the charge carriers move, a 0.25 T magnetic field is generated, which distorts the charge carriers' magnetic field. A magnetic force called the Lorentz force changes the direction in which charges move. This disturbance of the magnetic flow of the charge carriers leads to the deflection of positively charged holes to one side of the plate and negatively charged electrons to the other, resulting in a positive potential difference of 0.04 V (The Hall voltage). Because of the positive Hall voltage, the synthesised composites behave like p-type semiconducting materials this agrees with (Deshmukh *et al*., 2015; Nakazawa, *et al*., 2014). The ionic conductivities (electrical conductivity due to the motion of ionic charge) for rGO, $Pb_{0.4}:rGO_{0.6}$, and $Pb_{0.6}:rGO_{0.4}$ composites were determined to be 0.001341, 0.002368, and 0.002745 $\Omega^{-1}m^{-1}$. The average Hall coefficient (R_H) values for the rGO, $Pb_{0.4}:rGO_{0.6}$, and $Pb_{0.6}:rGO_{0.4}$ composites, respectively, are 3.12×10^3 m^3/C, 2.57×10^3 m^3/C, and 2.88×10^3 m^3/C.

The positive average Hall coefficients of the composites indicate p-type carrier conductivity. With increasing dopants, the variation in electrical conductivity was significantly influenced by the grain size of the doped composite. As the doping concentration increases, the crystallinity continuously increases, resulting in a more linear structure with larger grains. Larger grains could improve the carrier flow across the lattice and decrease the trap carrier density, which would increase conductivity, this agrees with (Nakazawa, *et al*., 2014; Siamak, *et al*., 2015). The network of rGOs act as a scattering center which experienced defect formation due to agglomeration, which may increase the possibility of trap states capable of capturing large numbers of free carriers exposed to conduction. After trapping mobile carriers, the carrier traps in $Pb_{0.4}:rGO_{0.6}$ and $Pb_{0.6}:rGO_{0.4}$ composites become electrically charged, lowering the potential energy barrier that prevents charge carrier mobility and increasing the amount of free carriers accessible for conduction, as a results increases the conductance of $Pb_{0.4}:rGO_{0.6}$ and $Pb_{0.6}:rGO_{0.4}$ composite.

CONCLUSION

In conclusion, the SEM image of $Pb_{0.4}:rGO_{0.6}$ and $Pb_{0.6}:rGO_{0.4}$ composite reveals how the surface coalescence breaks down with increasing dopant concentration as a result of slight growth in the number of grain boundaries. However, due to the fact that every samples were synthesised under the same conditions, regardless of the amount of doping, every doped composite had a very similar microstructure and surface morphology. The rGO, $Pb_{0.4}:rGO_{0.6}$, and $Pb_{0.6}:rGO_{0.4}$ have band gaps of 1.4 eV, 1.6 eV, and 1.8 eV, respectively. The ionic conductivities (electrical conductivity due to the motion of ionic charge) for rGO, $Pb_{0.4}:rGO_{0.6}$, and $Pb_{0.6}:rGO_{0.4}$ composites were determined

to be 0.001341, 0.002368, and 0.002745 $\Omega^{-1}m^{-1}$. The average Hall coefficient (R_H) values for the rGO, $Pb_{0.4}{:}rGO_{0.6}$, and $Pb_{0.6}{:}rGO_{0.4}$ composites, respectively, are 3.12×10^3 m^3/C, 2.57×10^3 m^3/C, and 2.88×10^3 m^3/C.

ACKNOWLEDGMENTS

REFERENCES

Alpha, M., Uno, U.E., Isah, K.U. and Ahmadu. (2019). Structural and Electrochemical Properties of AgxSnO1-x/G (0.3≤x≤0.4) Composite Electrode. European Journal of Scientific Research. 15, 14, 479-488

Daniel, T.O Uno, E.U., Isah, K.U. and Ahmadu, U. (2020). Tuning of SnS Thin Film Conductivity on Annealing in an Open Air Environment for Transistor Application. East European Journal of Physics, (2), 94-103

Deshmukh, G.D., Patil, S.M. and Pawar, P.H. (2015). Optical properties of thin Bi2Te3 films synthesized by different techniques. Journal of Chemical, Biological and Physical Sciences, 5, 2769.

Ilican, I., Caglar, Y. and Caglar, M. (2008). Preparation and characterization of ZnO thin films deposited by sol-gel spin coating method. Journal of Optoelectronics and Advanced Materials, 10 (200), 2578.

Jeyaprakash, B.G., Ashok, K.R., Kesavan, K and Amalarani, A. (2010). Synthesis and Some of Structural Characterisation of Nano Particles CdO Thin Film. American Journal of Science, 6

Kasap, S. and Capper, P. (2017) Handbook of electronic and photonic materials. Springer, Berlin 2nd edition

Largeot, J.C., Portet, C., Chmiola, J., Taberna, P.L., Gogotsi, Y. and Simon, P. (2008). Confinement, desolvation and electrosorption effects on the diffusion of ions innanoporous carbon electrode. Journal of American Chemical Society. 130, 2730.

Nakazawa, K., Itoh, S., Matsunaga, T., Matsukawa, Y., Satoh, Y. and Abe, H. (2014). Effect of dislocation and grain boundary on deformation mechanism in ultrafine- graine interstitial- free steel. Material Science and Engineering. 63, 012125

Mathias, S., Philipp, K., Vanya, D., and Tino, H. (2016). Optical Hall effect-model description. Journal of the Optical Society of America A, 33, 8, 1553-1568

Martinelli, A., Palenzona, A., Putti, M. and Ferdeghini, C. (2009). Microstructural transition in 1111 Oxy-Pnictides. J.W.Lynn, Pengcheng Dai Physica. C469.

Mukherjee, A. and Mitra, P. (2015). Structural and optical characterisation of SnS thin film prepared by SILAR. Material Science-Poland, 33, 847. https://doi.org/10.1515/msp-2005-0118

Pandolfo, A.G. and Hollenkamp, A.F. (2006). Carbon properties and their role in supercapacitors. Journal of Power Sources.; 11, 157-160.

Rajyalakshmi, T., Pasha, A., Khasim, S., Lakshmi, M. and Imran, M. (2020). Synthesis, characterization and Hall‑effect studies of highly conductive polyaniline/graphen nanocomposites. Applied Sciences (2020) 2:530. https://doi.org/10.1007/s42452-020-2349-4

Siamak, P.J., Alagarsamy, P., Boon, T.G., Hong, N.L. and Nay, M.H. (2015). Influence of particle size on performance of Nickel nanoparticles-based supercapacitor. RSC Advances. 5, 14010- 14019.

Skoog, D.A., West, D.M., Holler, F.J. and Crouch, S.R. (2016). Principles of Instrumental Analysis, Seventh Edition. USA: Cengage Learning.

Uwe, H. and Neil, G. (2011). The Scherrer equation versus the Debye-Scherrer Equation. Nature Nanotechnology, 6, 534.